ChemComm

COMMUNICATION

View Article Online
View Journal | View Issue



Cite this: *Chem. Commun.*, 2022, **58**, 9642

Received 15th June 2022,
Accepted 27th July 2022

DOI: 10.1039/d2cc03360g

rsc.li/chemcomm



# Dual-channel lanthanide-doped nanoprobe for reliable multi-signal ratiometric detection of $H_2S$ in whole blood†

Zheng Wei,‡§[a] Tianqi Cao,‡[a] Luoyuan Li,[b] Xingjun Zhu,[c] Jing Zhou*[a] and Yuxin Liu *[ad]

**Wavelength-dependent absorbance of blood has impeded the development of fluorescence biodetection in whole blood. Here, by replacing the fluorescence working signal with a temperature signal, reliable $H_2S$ detection was performed in samples of whole blood. The developed system was based on a dual-channel lanthanide-doped nanoprobe, which further allowed precise sero-diagnosis of acute pancreatitis.**

Ratiometric fluorescent nanoprobes have been intensively studied and widely used in the biodetection field as they can provide reproducible results in a short testing period. A typical ratiometric fluorescent nanoprobe should include both working and reference emissions, and construct a linear relationship between the ratio of emissions and the concentration of analytes.[1] To avoid the influence of the working emission on the reference emission, they are generally designed to be at different wavelengths. This design, however, introduces another delicate chain for biodetection in whole blood samples. Due to its chemical complexity, whole blood shows various optical transmittances at different wavelengths,[2] resulting in uneven extinctions of the working and reference emissions, and thereby causing false results.[3] Therefore, minimizing the influence of the wavelength-dependent absorbance of whole blood is a priority for achieving further developments of fluorescent nanoprobes.

For this purpose, recent work has aimed at constructing nanoprobes with working and reference emissions at the same wavelength.[4,5] However, it depends on the different lifetimes of the two emissions, which poses challenges to designing the probe and requires a specific time-gated technique to resolve them. As a result, a user-friendly method would be more favorable and needed to address this issue. One straightforward idea is to replace one of the emissions with a signal that is influenced less by the absorbance of whole blood and other biological conditions.[6] More importantly, it should be orthogonal to the other fluorescence signal, *i.e.*, the two signals should be made independent and free of interference from each other.[7] Comprehensive considerations have indicated temperature to be an ideal signal for this strategy and that a temperature signal should be incorporated into the design of fluorescent nanoprobes.[8]

Herein, a dual-channel lanthanide-doped nanoprobe was designed to produce fluorescence and temperature signals under the same light excitation. A lanthanide-based $NaErF_4$@$NaLuF_4$ nanophosphor, with a short-wave infrared (specifically 1550 nm-wavelength) emission, was chosen as the fluorescent core, while the Cu-based metal–organic framework HKUST-1 was used as the $H_2S$-responsive photothermal shell (Fig. 1a). In the detection process, $Cu^{2+}$ in HKUST-1 reacted with $H_2S$ in the sample. This reaction formed CuS, generating heat under near-infrared laser irradiation as a result of localized surface plasmonic resonance and thereby producing the temperature working signal (Fig. S1, ESI†). Meanwhile, the $NaErF_4$@$NaLuF_4$ provided the reference fluorescence emission. Due to the CuS displaying weak absorbance in the short-wave infrared range and due to the short-wave infrared fluorescence of $Er^{3+}$ being not thermally sensitive according to previous reports,[9] the temperature working signal and fluorescence reference signal were orthogonal as expected.

To confirm the applicability of this design, the $NaErF_4$@$NaLuF_4$ nanophosphor was prepared and then coated with an

[a] *Beijing Key Laboratory for Optical Materials and Photonic Devices & Department of Chemistry, Capital Normal University, 100048 Beijing, China. E-mail: jingzhou@cnu.edu.cn*
[b] *The Eighth Affiliated Hospital, Sun Yat-sen University, 518033 Shenzhen, Guangdong, China*
[c] *School of Physical Science and Technology, Shanghai Tech University, 201210 Shanghai, China*
[d] *Department of Biomolecular System, Max-Planck Institute of Colloids and Interfaces, 14476 Potsdam, Germany. E-mail: Yuxin.Liu@mpikg.mpg.de*

† Electronic supplementary information (ESI) available. See DOI: https://doi.org/10.1039/d2cc03360g

‡ These authors contributed equally to this work.

§ Current address: van't Hoff Institute for Molecular Sciences, HIMS-Biocat, University of Amsterdam, Science Park 904, 1098 XH Amsterdam, The Netherlands.

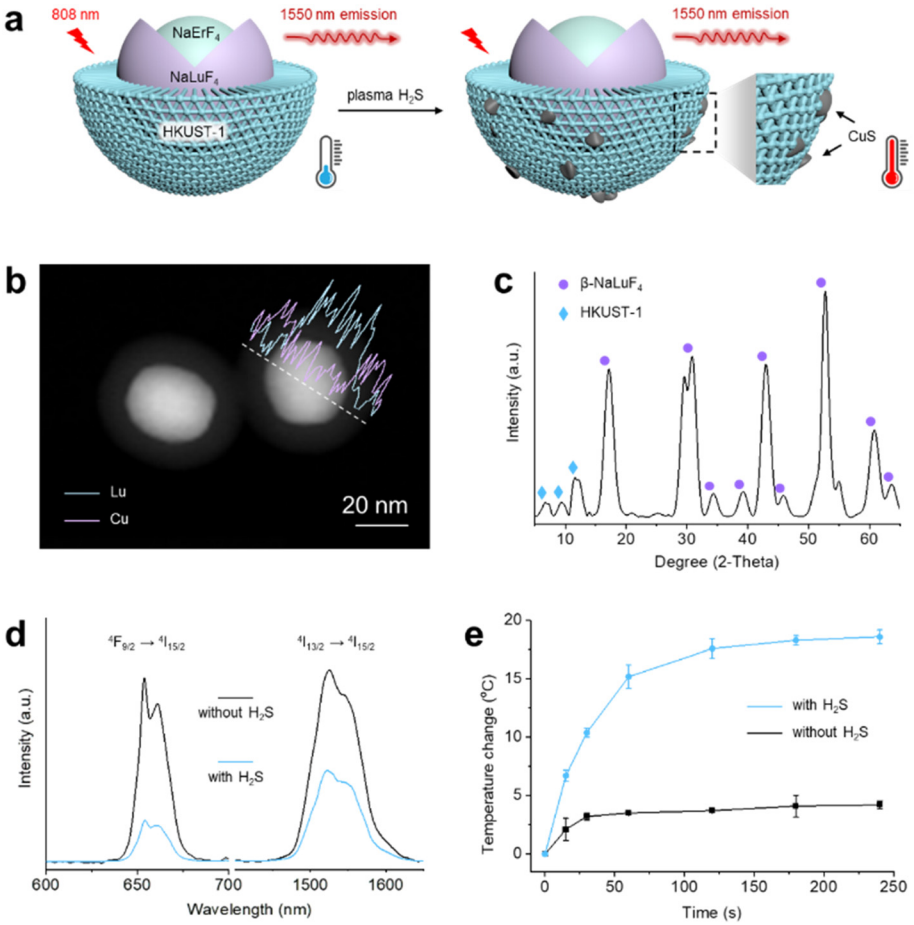


Fig. 1 Characterization. (a) Schematic presentation of the structure of Ln-CuMOF and its $H_2S$-response mechanism. (b) Scanning transmission microscopic image and X-ray energy dispersive line-scan results and (c) powder X-ray diffraction patterns of Ln-CuMOF. (d) Fluorescence spectra and (e) photothermal temperature curves of Ln-CuMOF in aqueous buffer solutions with and without $H_2S$. The excitation wavelength was 808 nm (1.5 W $cm^{-2}$). Data are represented as mean ± RSD ($n$ = 3).

HKUST-1 shell. The acquired scanning transmission electron microscopic image and X-ray energy dispersive line-scan results basically showed the core–shell nano-heterostructure (Fig. 1b). Powder X-ray diffraction patterns further indicated the presence of highly crystalline hexagonal-phase $NaLuF_4$ and HKUST-1 (Fig. 1c).[10] The as-prepared nanoprobe, abbreviated as Ln-CuMOF, was observed to be stable in water (Fig. S2, ESI†) and to display strong emissions at both wavelengths of 654 nm and 1550 nm under 808 nm-wavelength excitation, corresponding to, respectively, the $^4F_{9/2} \rightarrow {}^4I_{15/2}$ and $^4I_{13/2} \rightarrow {}^4I_{15/2}$ electron transitions of $Er^{3+}$ (Fig. 1d).[11,12] After the nanoprobe was allowed to react with $H_2S$ in neutral aqueous buffer, the intensities of both emissions decreased, due to the competitive photon absorbance of excitation of light, and the formed CuS further quenched the fluorescence at 654 nm through the inner filter effect (Fig. S3, ESI†). In contrast, under the same 808 nm-wavelength excitation, the temperature of the nanoprobe was increased by 18.6 °C after the reaction compared to an increase of $<5$ °C before the reaction (Fig. 1e). The results suggested that the Ln-CuMOF nanoprobe was successfully constructed with $H_2S$-responsive fluorescence and temperature channels.

Then, the $H_2S$ detection performance was evaluated with a specific focus on the anti-interference ability to the wavelength-dependent absorbance. $H_2S$ is an essential gaseous molecule that is involved in the occurrence and progression of various diseases. Therefore, the precise quantification of $H_2S$ in biological fluids, especially in whole blood, would benefit our understanding of many biological processes and would benefit biomedical diagnosis, and has therefore garnered considerable attention in the last decade; and many elegant optical methods to achieve such quantification have been developed.[13–15] However, due to the presence of coloration substances (*e.g.*, hemoglobin), whole blood shows strong absorbance in the visible range (Fig. 2a). Therefore, the working emission in the visible range could be subjected to significant extinction by the blood rather than by the target analytes, resulting in false positives in actual practice (Fig. 2b). This phenomenon was also observed in our case when the fluorescence at a wavelength of 654 nm was used as the working signal. In a colorless buffer solution, the calibration curve within the biological $H_2S$ concentration range was $Y = -2.97X + 1.24$ ($R^2$ = 0.994), but was significantly different, namely $Y = -3.33X + 0.76$ ($R^2$ = 0.998), in the presence

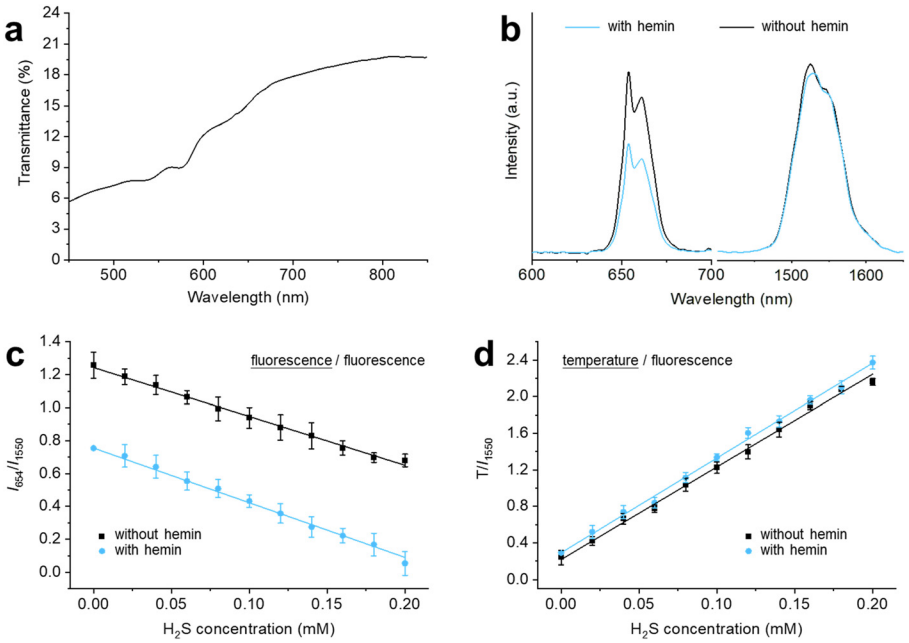


Fig. 2 Biodetection performance. (a) Absorbance spectrum of freshly collected whole blood. (b) Fluorescence spectra of Ln-CuMOF in aqueous buffer solutions with and without hemin. The excitation wavelength was 808 nm (1.5 W $cm^{-2}$). (c) Plots showing linear relationships between $I_{654}/I_{1550}$ and $H_2S$ concentration for the fluorescence/fluorescence method. (d) Plots showing linear relationships between $T/I_{1550}$ and $H_2S$ concentration for the temperature/fluorescence method. Data are represented as mean ± RSD ($n$ = 3).

of absorbance of blood. This difference indicated that in samples of whole blood, the tested concentration of $H_2S$ determined in this way would be mistakenly higher than its actual concentration. However, when the temperature was used as the working signal, the calibration curves were basically the same, namely $Y = 1.01X + 0.02$ ($R^2 = 0.994$) in the presence of the absorbance of blood and $Y = 1.04X + 0.03$ ($R^2 = 0.998$) in its absence, which suggested that the tested result determined in this way would be close to the actual concentration and thus reliable for measurements in samples of whole blood.

To further demonstrate the advantage of the multi-signal ratiometric method in actual practice, the acute pancreatitis (AP) mouse model was established as the disease model for serodiagnostic study. By performing a receiver-operating characteristic analysis, the diagnostic precision was determined quantificationally. For the serum sample test, both the fluorescence–fluorescence and temperature–fluorescence ratiometric methods showed outstanding levels of precision, specifically 99.3% and 97.8%, respectively, with these levels sufficient for actual biomedical practice ($\geq$ 95%). However, for the test using whole blood, the precision using the fluorescence–fluorescence method sharply decreased to 87.3% (Fig. 3a), and at this low level was the main contributor to the elevated false-positive rate, and was lower than that meeting essential medical requirements. In contrast, the temperature–fluorescence method maintained a high precision, specifically 95.5%, in whole blood (Fig. 3b), with this level of precision sufficient for medical applications and better than that obtained using the colorimetric method in a typical whole-blood test (65.4%, Fig. S4, ESI†).

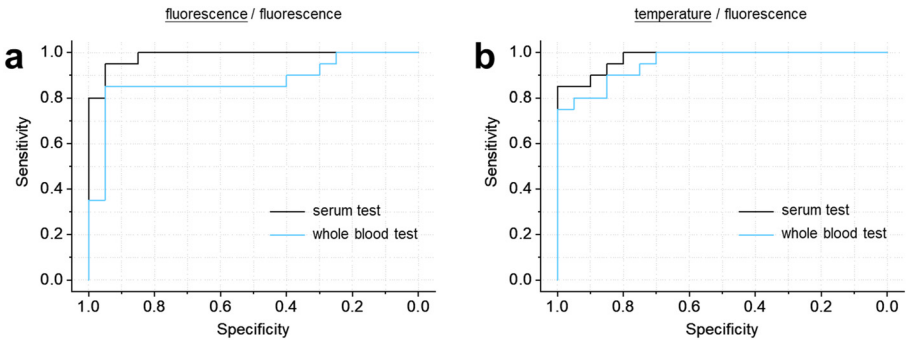


Fig. 3 Serodiagnostic study. Receiver-operating characteristic curves showing the probabilities of the assays correctly distinguishing between normal and AP cases based on the plasma $H_2S$ concentration in serum or whole-blood samples as determined using the (a) fluorescence/fluorescence method and (b) and temperature/fluorescence method.

 

In summary, based on the dual-channel lanthanide-doped nanoprobe Ln-CuMOF, a multi-signal ratiometric method was established for detecting $H_2S$ in whole blood samples. As the temperature working signal was free of any influence from the wavelength-dependent absorbance of whole blood, the temperature–fluorescence ratiometric method showed higher reliability than did the conventional fluorescence–fluorescence ratiometric method. The same result was also observed in an indicator-based serodiagnostic study. Therefore, the multi-channel fluorescent nanoprobe and as-proposed multi-signal ratiometric approach are expected to provide great opportunities for efficacious biodetection.

Y. L. conceived the project and wrote the original manuscript. Y. L. and J. Z. supervised the project, designed the methodology, and established the model for study, while J. Z., Y. L., L. L., X. Z., and Z. W. acquired the financial support. T. C. synthesized and characterized the nanoparticle. Z. W. performed the detection *in vitro*. Y. L. and X. Z. performed the experiments involving small animals. Z. W. and Y. L. performed the serodiagnostic experiment and analysed the results under the guidance of L. L. All authors contributed to the editing of the submitted and revised manuscripts.

The authors are grateful for financial support from the National Natural Science Foundation of China (92159103, J. Z.; 82001945, X. Z.; 61905130, L. L.), the Beijing Municipal Education Commission Outstanding Young Individual Project (CIT&TCD201904082, J. Z.), the Shanghai Pujiang Program (20PJ1410700, X. Z.), the Youth High-level Talent Project of Capital Normal University (20530810024, J. Z.), the High-level Talent Introduction Program at The Eighth Affiliated Hospital of Sun Yat-sen University (GCCRCYJ039, L. L.), the China Scholarship Council scholarship (202008110184, Z. W.), the Max-Planck Society (Y. L.), and the Yanjing Young Scholar Program of Capital Normal University (J. Z.)

## Conflicts of interest

There are no conflicts to declare.

## Notes and references

1 L. L. Wu, C. S. Huang, B. Emery, A. C. Sedgwick, S. D. Bull, X. P. He, H. Tian, J. Yoon, J. L. Sessler and T. D. James, *Chem. Soc. Rev.*, 2020, **49**, 5110–5139.
2 D. K. Sardar and L. B. Levy, *Lasers Med. Sci.*, 1998, **13**, 106–111.
3 G. S. Hong, J. C. Lee, J. T. Robinson, U. Raaz, L. M. Xie, N. F. Huang, J. P. Cooke and H. J. Dai, *Nat. Med.*, 2012, **18**, 1841.
4 S. M. Cheng, B. Shen, W. Yuan, X. B. Zhou, Q. Y. Liu, M. Y. Kong, Y. B. Shi, P. Y. Yang, W. Feng and F. Y. Li, *ACS Cent. Sci.*, 2019, **5**, 299–307.
5 X. C. Qiu, Q. W. Zhou, X. J. Zhu, Z. G. Wu, W. Feng and F. Y. Li, *Nat. Commun.*, 2020, **11**, 4.
6 Y. X. Liu, Z. Wei, X. Q. Liao and J. Zhou, *Acc. Mater. Res.*, 2020, **1**, 225–235.
7 Y. X. Liu, X. J. Zhu, Z. Wei, W. Feng, L. Y. Li, L. Y. Ma, F. Y. Li and J. Zhou, *Adv. Mater.*, 2021, **33**, 2008615.
8 Y. X. Liu, Z. Wei and J. Zhou, *Biosens. Bioelectron.*, 2019, **140**, 57–63.
9 Y. X. Liu, Z. Wei, J. Zhou and Z. F. Ma, *Nat. Commun.*, 2019, **10**, 5361.
10 O. Shekhah, H. Wang, S. Kowarik, F. Schreiber, M. Paulus, M. Tolan, C. Sternemann, F. Evers, D. Zacher, R. A. Fischer and C. Woll, *J. Am. Chem. Soc.*, 2007, **129**, 15118.
11 Y. Song, M. Lu, G. A. Mandl, Y. Xie, G. Sun, J. Chen, X. Liu, J. A. Capobianco and L. Sun, *Angew. Chem., Int. Ed.*, 2021, **60**, 23790–23796.
12 Z. Wang, X. Qiu, W. Xi, M. Tang, J. Liu, H. Jiang and L. Sun, *Sens. Actuators, B*, 2021, **345**, 130417.
13 W.-M. He, Z. Zhou, Z. Han, S. Li, Z. Zhou, L.-F. Ma and S.-Q. Zang, *Angew. Chem., Int. Ed.*, 2021, **60**, 8505–8509.
14 M. Dulac, A. Melet and E. Galardon, *ACS Sens.*, 2018, **3**, 2138–2144.
15 X. Li, T. Zhang, J. Yu, C. Xing, X. Li, W. Cai and Y. Li, *ACS Appl. Mater. Interfaces*, 2020, **12**, 40702–40710.